ADVANCED MATERIALS

Advanced Zeolite Materials Science**

By Geoffrey A. Ozin,* Alex Kuperman, and Andreas Stein

Molecular Electronics
Quantum Dots/Chains
Zeolite Electrodes, Batteries and Membranes
Nonlinear Optical Materials
Chemical Sensors
Zeolite-Polymer Composites

1. Introduction

In today's search for smaller, faster, more selective and efficient products and processes, the ability to engineer well defined spatial microarrangements of pure substances and composite materials is becoming pivotal in creating new molecular level electronic, optical and magnetic devices. One attractive method for assembling and maintaining controlled microstructures is to use solid host lattices that serve as templates within which a guest stucture of nanometer architecture can be assembled. It is the thesis of this paper that zeolites as microporous molecular electronic materials with nanometer dimension window, channel and cavity architecture represent a "New Frontier" of solid state chemistry with great opportunities for innovative research and development.

Since the first synthetic preparation of zeolites by *Barrer* in the 1940's[1] these aluminosilicate materials have been used in large quantities for hydrocarbon conversion, size/shape selective heterogeneous catalysis, gas separation and purification, as well as for ion exchange, dessication and sorbing processes.[2] Although only few zeolite compositions are used in large scale processes, the number of specifically tailored zeolite structures and modifications has increased immensely within the last decade, along with the number of publications concerning new physicochemical characterization techniques for these framework materials. In zeolite characterization X-ray and neutron diffraction, solid state magic angle spinning (MAS) NMR and FT mid and far infrared spectroscopy have proven particularly useful.[3] Combined, these methods provide comprehensive information about zeolite physicochemical properties and allow one to monitor transformations of and within the zeolite lattice.

Much zeolite research and development is still aimed at the traditional uses mentioned above. However, within the last few years considerable effort has been directed at new uses of zeolites as advanced materials. For example, in the field of solar energy conversion technology a spatially well organized molecular system is required that models photosynthetic mechanisms, thereby allowing redox reactions to proceed efficiently along desired paths. Other potential applications include zeolite electrodes and electron relays, zeolite batteries, zeolite fast ion conductors, intrazeolite semiconductors, zeolite chemical sensors, zeolite imaging and data storage materials, zeolite lasers and displays, as well as zeolite composites to form permselective membranes or thin films.

Most of the traditional and advanced applications for zeolites are based on the ability of these open crystalline structures to selectively incorporate and exchange both charged and neutral species within the void spaces and interconnecting channels on a molecular scale. In order to appreciate the unique features of zeolites it is necessary to take a brief look at their structures and compositions. Conventional zeolite structures are composed of three dimensional networks of SiO_4 and AlO_4 tetrahedra in which a unit negative charge is associated with each AlO_4 tetrahedron. This charge must be counter-balanced by a positive inorganic or organic ion. Depending on the type of connection between tetrahedral building blocks, linear or pseudo-linear channels may be formed with diameters ranging from 4.2 to 7.4 Å. In other structural types cages are formed with diameters of 6.4 to 12 Å and window sizes from 2.3 Å (6-ring) to 13 Å (18-ring). Figure 1 illustrates some typical examples of commonly encountered zeolite structures.

Isomorphous replacement of framework $Al^{3\oplus}$ and $Si^{4\oplus}$ by other elements such as $Ga^{3\oplus}$, $Ge^{4\oplus}$, $B^{3\oplus}$, $P^{5\oplus}$ as well as enrichment in framework $Si^{4\oplus}$ can be readily achieved. Most notable in this context are synthetic strategies that lead to highly or completely siliceous zeolites like ZSM-5 and silicalite as well as a new generation of molecular sieves exemplified by the aluminophosphates (ALPO's), silicoaluminophosphates (SAPO's) and their metal doped analogues denoted MAPO's and MAPSO's, where, for example, M = Li, Be, Mg, Cr, Mn, Fe, Co or Zn. The lattice of silicalite is neutral in contrast to the positively charged SAPO lattice which is negatively charged when $P^{5\oplus}$ has been partially replaced by $Si^{4\oplus}$, allowing for cation exchange. Recently a novel positively charged SAPO lattice has been synthesized in which $Al^{3\oplus}$ has been partially re-

[*] Prof. G. A. Ozin, A. Kuperman, A. Stein
Lash Miller Chemistry Department
University of Toronto
80 St. George Street, Toronto, Ontario M5S 1A1 (Canada)

[**] The generous financial support of the Natural Science and Engineering Research Council of Canada's Operating and Strategic Programmes, Union Carbide, Tarrytown, NY, USA, and Alcan, Canada, is gratefully appreciated. *A. S.* is deeply indebted to NSERC for a science graduate scholarship. Preprints of manuscripts from Professors *Tom Mallouk* and *Thomas Bein* assisted us greatly in the writing of this review paper. We also thank all our coworkers at the University of Toronto for many enlightening suggestions and discussions during the course of our research in advanced zeolite materials science.

placed by $P^{5\oplus}$, now permitting the less common mode of anion exchange.[4] The majority of the new generation molecular sieves crystallize with an encapsulated organic template, usually a charge balancing alkylammonium ion. The template can be effectively removed by controlled calcination procedures to yield the protonated analogue of the sieve which can often be subsequently ion-exchanged for other cationic guests. A wide variety of guests have been encapsulated in zeolites ranging from atoms, ions, metal clusters and salts to coordination complexes and organometallics. Until very recently this kind of inclusion chemistry has been driven mainly by the science and technology of specific molecule adsorption and diffusion, molecular sieving and chemical/catalytic transformations, usually taking advantage of restricted geometry environments.

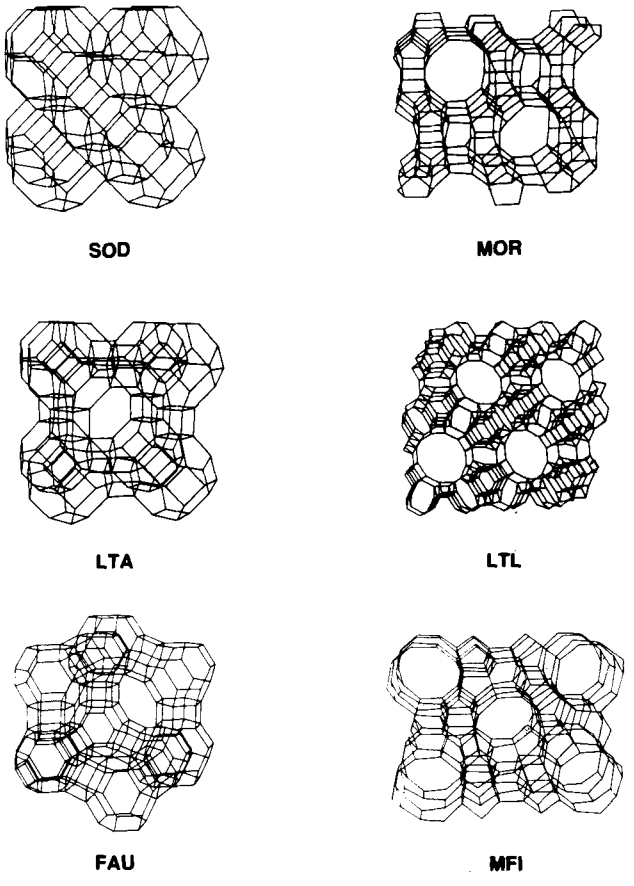

Fig. 1. Some typical zeolite structures: (SOD) sodalite, (LTA) Linde type A zeolite, (FAU) faujasite: zeolites X or Y, (MOR) mordenite, (LTL) Linde type L zeolite, and (MFI) ZSM-5 [49].

In view of the impressive range of zeolite framework structures and element substitution, rich extraframework cation modification, variety of encapsulated guests, tunable Brønsted acidity and lattice oxygen basicity, as well as the controllable hydrophobic/hydrophilic character, one can envisage that future innovations in the field will likely occur at the interface between zeolite science, solid state chemistry and molecular electronics.

2. Intrazeolitic Semiconductors

While the physical properties of materials are fairly well understood on both the molecular and bulk levels, the quantum size regime encompassing microscopically structured solids from 5 to 100 Å is the subject of much current research.[5] Particles of this size display electrical, optical and magnetic properties that are essentially independent of their chemical composition, but are related instead to their extremely small dimensions.

The tremendous present interest in ultrasmall semiconductor particles can be considered to derive from the original notion of artificially layered structures known as semiconductor superlattices, and from the exciting optical and electrical properties that such quasi-two dimensional (2D) electron systems offer. The formation of modulated chemical composition layers of this kind with a periodicity larger than the natural lattice spacing but smaller than the de Broglie wavelength of electrons of the semiconductor components, allows the realization of band gap engineering, heterojunctions, composition and doping superlattices, multiple quantum well (MQW) lasers, high electron mobility transistors, (HEMT's) non-linear optical (NLO) superlattices and optical transistors (transphasors) to name just a few applications.[6a]

Theoretical considerations have indicated that quantum size effects are significantly enhanced when the dimensionality of a quasi-2D semiconductor is further reduced. For example, strongly enhanced electron mobilities and resonant tunneling have been predicted and recently observed in the case of quantum wires and quantum boxes. Fundamental alterations in their electronic/optical properties are expected by the novel 1D and 0D quantum confinement of excitons and the modified density of states.[6b]

A major challenge in the synthesis of spatially resolved materials is the reproducible fabrication of microscopically organized semiconducting solids having quasi-1D and quasi-0D electronic/optical properties. Common methods for producing quantum microstructures include molecular beam epitaxy (MBE), metal-organic chemical vapor deposition (MOCVD), electron beam lithography and reactive ion etching.[6b, 7] As a way to avoid the minimum size limitations of electron-beam lithography, which are typically ca. 0.02 μm,[6b, 8] quantum size particles have been prepared and studied in liquid suspensions, micelles, glasses, and zeolites.[9] Host matrices like zeolites reduce the interchain and interlayer perturbation often encountered in other low dimensional solids.[10] Zeolites have an advantage over the other matrices listed, because they permit the ordered inclusion of particles with very small dimensions and a very uniform size distribution. By using zeolites of different architecture the spatial arrangement of

ADVANCED MATERIALS

the quantum size particles can be controlled and cluster growth constrained to molecular dimensions. At the same time the zeolite lattice provides a stabilizing medium because of kinetic impediments imposed on further agglomeration processes. Modification of framework charge density and electric field gradients provides extra flexibility for designed perturbation of the entrapped semiconductor characteristics (i.e. a semiconductor-support effect).

In what follows we describe some pioneering experiments aimed at producing well defined semiconductor quantum dots and semiconductor superlattices in various zeolite hosts.

3. Quantum Dots and Semiconductor Superlattices

An intriguing new avenue of advanced zeolite materials science involves the synthesis and stabilization of isolated sub-colloidal dimension intrazeolite semiconductor aggregates. As the pore filling of the zeolite is increased a percolation threshold is reached. At this point a semiconductor supercluster lattice is created by the 3D interconnection of intrazeolite quantum dots to yield materials with properties intermediate between those of discrete, "molecule-like" semiconductor clusters and bulk semiconductors. Experiments of this kind have been reported for narrow band gap semiconductors like CdS, CdSe and PbS.

Herron et al.[11, 12] have recently succeeded in incorporating semiconductor materials inside zeolites X, Y, and A. Such particles are referred to as "quantum dots" in the terminology of finely divided semiconductors. Excitons in these materials are confined in three dimensions. Due to the small size and reduced dimensionality of the occluded semiconductors, their electronic properties are altered. Absorption edge energies of confined CdS microcrystals are larger than in the bulk semiconductor,[8] so that spatial confinement of these materials allows for band gap adjustment. As the semiconductor cluster size decreases the excited-state relaxation dynamics are also influenced considerably by the host and its interface with the semiconductor.[11]

CdS particles were synthesized inside the zeolite A, X or Y framework by exposing the calcined $Cd^{2\oplus}$ ion exchanged zeolite to flowing hydrogen sulfide at 100°C. X-ray diffraction (XRD) and extended X-ray absorption fine structure (EXAFS) results revealed that discrete, cubic $(CdS)_4$ clusters (interpenetrating Cd and S tetrahedra) with a Cd-S bond length of 2.47 Å were formed strictly inside the smaller sodalite cages, where a stabilizing interaction between the cluster and framework oxygen of the double 6-rings was possible (Fig. 2). At low $Cd^{2\oplus}$ loading these clusters were isolated but formed an interconnecting extended supercluster structure as the cluster concentration increased. In this case the Cd-Cd separation between adjacent sodalite cages was ca. 6 Å, allowing for long-range interactions. It has been suggested that the supercluster was formed by a percolative process with a percolation threshold of 4 ± 1 wt%. At higher loading $(CdS)_4$ clusters must populate adjacent sodalite units. The highest CdS loading that was achieved (ca. 23 wt%) filled nearly all sodalite cages. The CdS clusters, as well as PbS clusters encapsulated in zeolites[13] were stable for at least six months in a dry, oxygen-free environment.

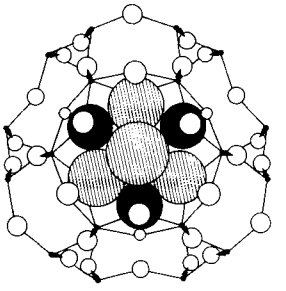

Fig. 2. Representation of the Cd_4S_4 cube inside the sodalite unit [12, 14].

Optical absorption near 290 nm characterized these ultrasmall semiconductor aggregates. Discrete $(CdS)_4$ cubes began to interconnect at higher loading densities to create a supercluster structure displaying optical absorption near 350 nm. The latter absorption is likely due to an exciton transition similar to that found in 25–30 Å colloidal CdS particles. Above the percolation threshold the absorption spectra became independent of the CdS concentration. *Wang* and *Herron*[11] studied the photoluminescence and relaxation dynamics of the superclusters. The three different emission bands observed were attributed to defect luminescence: a yellow/green band due to Cd atoms, a red band caused by sulfur vacancies, and a blue band due to shallow donors, which was probably also sulfur related. Defects like these break up the supercluster into smaller units of irregular sizes. The authors believe that the effect of the surrounding matrix on the absorption spectra of the semiconductor clusters was small, and did not alter the conclusions drawn about quantum size effects.

It has been found that partial occupancy of zeolite sites by $Cd^{2\oplus}$ produces CdS supercluster size distributions in the zeolite lattice rather than the possibly more desirable homogeneous semiconductor superlattice. Only in the case of zeolite X with the highest ion-exchange capacity, can the maximum loading of 25 wt% CdS be achieved which is close to the 27 wt% required for filling available sodalite cages. A similar investigation by *Moller* et al.[14] involved the incorporation of quantum size CdSe clusters in zeolite Y, which are of interest in the study of photosensitized electron-transfer reactions utilized for solar energy conversion and photocatalysis. A mixture of CdSe and probably helical Se chains was obtained.

The early results from these systems support the idea that semiconductor loaded zeolites have the potential to be tuned from 0D quantum dot type structures to 3D superlattice structures, the spatial arrangement and distribution of which are controlled by the templating action and framework architecture of the zeolite host.

4. Silver Sodalites: Novel, Optically Responsive, Packaged Silver Salts

β-Cages are the building blocks for several classes of zeolites. The zeolites composed exclusively of β-cages, called sodalites, have been studied mainly as model compounds for larger zeolite systems. Because of their small entrance windows (2.3 Å diameter) which block the passage of most molecules, sodalites have not been used in applications involving catalysis or gas separation. However, closer inspection leads to the realization that the sodalite lattice forms a convenient matrix for encapsulation of a variety of guests. By controlling the loading of the trapped species, it is possible to form cluster and extended supercluster structures in the quantum size regime, similar to the semiconductor superclusters described in the previous section. One important advantage of sodalites is that the lattice is comprised entirely of close-packed sodalite cages, rather than the coexisting sodalite and supercages of other zeolite hosts, thereby permitting direct or through-bond interaction between guests in *all* cages. In addition, the presence of guest-anions make sodalites unique. These can be used as internal reagents (e.g. for intra-sodalite cage redox reactions) and provide great flexibility in the composition of trapped species. By judicious selection of the anion and cation one can form packaged insulators and semiconductors as well as metals within the sodalite framework. Control of the guest-concentration in sodalites facilitates the transition above a percolation threshold (PT) from molecular type species to expanded bulk materials, as illustrated in Figure 3.

One facet of Figure 3 has recently been studied in our laboratory.[15] A range of novel silver sodalites have been synthesized. These solid state microstructures are viewed as "packaged" silver salts comprised of nanoassemblies of silver cations tetrahedrally organized with various charge balancing anions. A collection of physicochemical characterization techniques have been employed to interrogate

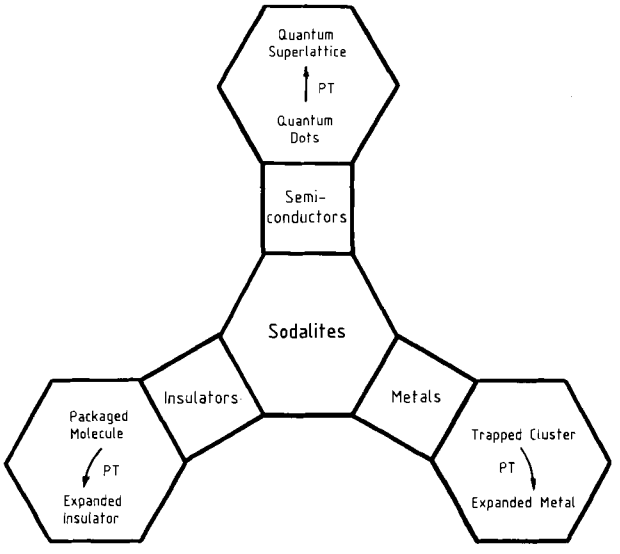

Fig. 3. Origami diagram showing the transitions between isolated and expanded insulators, semiconductors and metals that can potentially be formed within sodalites (PT = percolation threshold) [15].

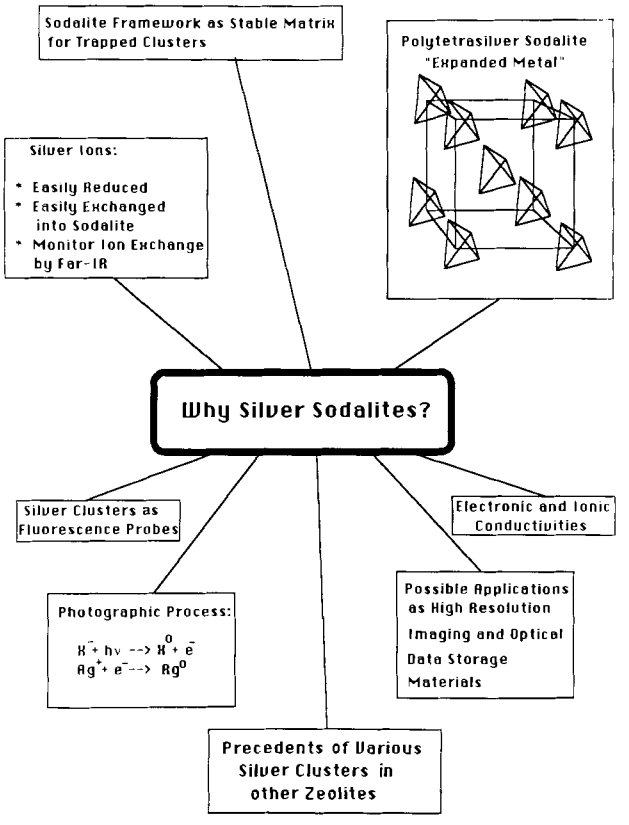

Fig. 4. Summary of the attractive features of silver sodalites in solid state chemistry [15].

the structure and properties of the parent silver sodalites, as well as the chemical and physical transformations of the encapsulated silver salts that relate to a number of transducer effects. An interesting question in these materials concerns intercavity communication between aggregates of the entrapped silver salt and the connection of their properties with those of the analogous bulk phase material (such as electronic transport, photoconductivity, photoaggregation and photoluminescence). Intracavity redox processes that produce encapsulated silver clusters and expanded-metal-superlattice phenomena above the PT loading level are also intriguing avenues of enquiry within the silver sodalite family of materials. In this section we will briefly describe the synthesis and characterization of a few key silver sodalites and examine their possible utilization in high resolution imaging/printing and high density data storage applications. A summary of some of the attractive features of silver sodalites in solid state chemistry is presented schematically in Figure 4.

ADVANCED MATERIALS

Sodalites with sodium cation guests are readily synthesized by hydrothermal reactions of silicate and aluminate sources (e.g. kaolin; or silica gel and sodium aluminate) with the appropriate anion salt in concentrated NaOH solutions. Sodium ions are exchanged for silver ions in a silver salt melt, or in some instances, in a silver salt aqueous solution. The framework structure is generally maintained after exchange, as confirmed by powder X-ray diffraction studies and mid-IR spectroscopy of the framework vibrations. The silver sodalites prepared to-date in our laboratory are listed in Table 1. The silver exchange process is conveniently monitored by the accompanying intensity changes of diagnostic sodium and silver ion translatory modes in the far-IR as well as by shifts in the frequencies of far-IR anion translations.

Table 1. Silver sodalites [15, 48].

Sodalite Type	Reason for Study
Ag, Cl–SOD	Analogues to photochromic and cathodochromic sodalites
Ag, Br–SOD	Similarities with photographic process
Ag, I–SOD	Occluded guest species are photoconductors, semiconductors, fast-ion conductors Study variation in properties down a group
Ag, S–SOD	Sensitization
Ag, Br, S–SOD	Photographic imaging
Ag, OH–SOD	Some hydroxide present in most hydrothermally prepared sodalites
Ag_6–SOD	Cages contain only three silver ions and no anion Occluded metal clusters Expanded metal Quantum size effects
Ag, CO_3–SOD	Intracage anion decomposition possible
Ag, HCO_2–SOD ≡ Ag, Fo–SOD	Redox switching
Ag, C_2O_4–SOD ≡ Ag, Ox–SOD	
Ag, ClO_4–SOD	
Ag, SO_x–SOD	
Na, Ag, X–SOD	Mixed cation systems to study silver concentration effects Tunable insulators /semiconductors (NaX: insulators; AgX: semiconductors, ion conductors)

Many of the silver sodalites prepared in these studies are novel materials. Interesting responses in color as well as luminescence properties were observed upon exposing several compositions to a variety of physical stimuli, including heat, light, pressure, moisture, X-rays and e-beams (Table 2). Some of the changes were reversible or semi-reversible.

The observed effects are related to the ease of silver reduction and the ability of the silver to form small clusters or expanded superclusters within the sodalite framework. In silver hydroxo-, formato- and oxalato sodalites this is facilitated by the intrazeolitic redox reactions (1)-(4). Reaction (4) can be effected both thermally and photolytically. Depending on the level of silver exchange, aggregates of the type $(Ag_nNa_{4-n})^{q\oplus}$, $n=0$ to 4, may be formed within the cages, where charge variations of q in the range $q=(4-n)$ to 4 can lead to the observed optical responses.

$$2Ag^{\oplus}(Z) + H_2O(Z) \longrightarrow 2Ag^0(Z) + 1/2\,O_2 + 2H^{\oplus}(Z) \quad (1)$$

$$2Ag^{\oplus}(Z) + OH^{\ominus}(Z) \longrightarrow 2Ag^0(Z) + 1/2\,O_2 + H^{\ominus}(Z) \quad (2)$$

$$2Ag^{\oplus}(Z) + HCO_2^{\ominus}(Z) \longrightarrow 2Ag^0(Z) + CO_2(Z) + H^{\ominus}(Z) \quad (3)$$

$$2Ag^{\oplus}(Z) + C_2O_4^{2\ominus}(Z) \longrightarrow 2Ag^0(Z) + 2CO_2 \quad (4)$$

The silver, oxalato-sodalite (Ag, Ox–SOD) system will be used as an illustrative example. The results of a full-profile Rietveld analysis of X-ray powder diffraction data for completely silver ion-exchanged Ag, Ox–SOD showed that the intracage Ag-Ag distances varied from 4.5 Å to ca. 6 Å, and intercage Ag-Ag distances from 4.5 to 4.9 Å, depending on the cage contents. These interatomic distances are too long for direct overlap of the silver orbitals but they are well within the range of through-bond interaction involving the sodalite framework. Such long range interactions would allow the formation of an expanded silver supercluster. From a unit cell size study of Na,Ag,Ox-sodalites with various silver loadings, together with transmission electron microscopy (TEM) and powder XRD data, it was determined that β-cage encapsulated $Na_n^{\oplus}Ag_{4-n}^{\oplus}$ moieties were distributed statistically throughout the sodalite lattice, in a solid-solution like manner as a function of n.

After aqueous silver exchange, Na,Ag,Ox-sodalites are white. Following thermal treatment at a temperature allowing for intrazeolite oxalate redox reaction (4), the materials

Table 2. Qualitative responses of silver sodalites to various physical stimuli [15, 48].

Barochromic:

White Ag, OH–SOD or Ag, HCO_2–SOD samples darken upon application of pressure.

Hydrochromic:

Ag, OH–SOD undergoes a reversible color change upon dehydration.

Photochromic:

Color changes and/or sample darkening can be produced by irradiation of Ag, Ox–SOD, Ag, OH–SOD, $AgCO_3$–SOD, Ag, HCO_2–SOD and sulfur-doped silver sodalites with various light sources.

Thermochromic:

Na, Ag, Ox–SOD, Ag, OH–SOD and sulfur-doped silver sodalites undergo various color changes upon heat treatment.

X-ray sensitivity:

White Ag, Ox–SOD turns yellowish green upon exposure to X-rays.

Fluorescence changes:

Heat, light and X-rays can induce Na, Ag, Ox–SOD samples to fluorescence under UV-light.

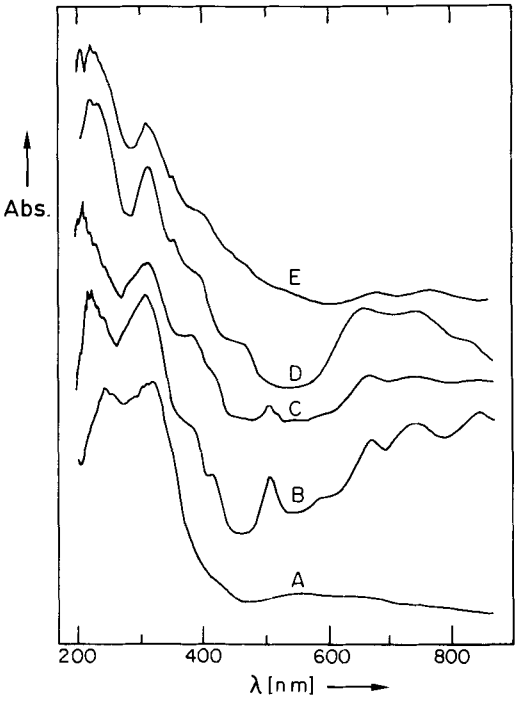

Fig. 5. UV-visible reflectance spectra of oxalato sodalites. A) Na,Ox-SOD (white); B) Na,Ag,Ox-SOD (1 Ag/unit cell), (light grey); C) Na,Ag,Ox-SOD (2 Ag/unit cell), (bluish grey); D) Ag,Ox-SOD (green); E) Ag,Ox-SOD, exposed to sunlight for four days (pale yellowish green). Samples B–E had been synthesized by $AgNO_3$-melt exchange at 230°C [15, 48].

absorb light in the UV and visible regions, the absorption spectrum depending on the silver concentration (Fig. 5). Concentration effects are also exhibited by the position of the most intense emission bands. Variations in both the identities of trapped silver clusters and the unit cell sizes could be responsible for the shifts in transition energies.

The fate of the oxalate ion during thermal treatment was followed by thermogravimetric analysis coupled with mass spectrometry (TGA-MS), mid-IR spectroscopy and powder X-ray diffraction. A comparison of the results for sodium oxalato-sodalite and silver oxalato-sodalite indicated that the reduction potential of the cation directs the reaction mechanism. While in the silver oxalate sodalite the anion is oxidized to CO_2 with concomitant reduction of the silver ions, oxalate ion decomposition in the sodium oxalate sodalite produces CO and $CO_3^{2\ominus}$, with no redox reaction occurring. In Na,Ag,Ox-sodalites the degree of silver exchange can thus be used to control not only the optical and structural properties, but also the thermal behavior of the sodalite.

Although the number of electron equivalents involved in intracavity silver ion reduction was shown to be relatively small, the alterations in silver cluster optical properties that ensue are quite spectacular. As a result, the silver sodalites lend themselves to applications in high resolution imaging and optical data storage, because the regular close-packed framework structure can trap and stabilize clusters formed inside. During a write cycle these clusters can be manipulated by the physical or chemical treatments described above (Table 2) to change their optical properties and produce a mark on the sodalite samples. The presence or absence of an optically absorbing or fluorescing mark defines a binary state. The size of the mark is affected mainly by the silver distribution, the sodalite particle size and the writing mechanism employed. The sodalite may be in the form of a self-supporting pressed disk, suspended in another material (e.g. glass or polymer), or supported on a substrate as a thin film.[15]

5. Quantum Chains

The isolation of selenium chains with controlled lengths and conformations in a zeolite host provides an interesting opportunity to probe quantum size effects in a 1D semiconductor. This type of selenium falls into the category of a "quantum chain", and may comprise a system that can exhibit discrete energy levels within the bulk semiconductor band structure with quantization of electronic properties in one dimension. One can expect isolated selenium chains to bridge the behavior between atomic/molecular forms of selenium and the bulk semiconductor trigonal form. In this regard, some interesting structure-property questions arise concerning the effects of interchain interactions, spatial restrictions and confinement on chain conformation. Selenium is of interest, because it has an intermediate electrical conductivity with a negative coefficient of resistivity in the dark. It is markedly photoconductive and has uses in, for example, photoelectric devices and xerography.

Bogomolov et al.[16] stabilized single selenium and tellurium chains in the unidimensional mordenite channels by injecting Se or Te into the zeolite from a melt under pressure or by incorporating the chalcogenide in the mordenite channels by vapor phase absorption. Isolated Se chains in mordenite channels are strongly photosensitive.[17] Results from a quantitative X-ray microprobe analysis indicated that one trigonal (helical) Se or Te chain was present in each channel with a period multiple with that of mordenite. The important question of whether the Se chains were actually *included and isolated* within the zeolite was addressed by *Tamura* et al.[17] The Se uptake (23%) in mordenite agreed with an estimate based on the assumption that the bond length of a single occluded Se chain is 2.32 Å and that the chain forms the same helical structure as in the crystalline trigonal Se. High-resolution electron micrographs of mordenite, into which Se had been inserted[10] provided further evidence of the inclusion of Se chains. This analytical technique, together with EXAFS, ^{77}Se MAS-NMR, and optical spectroscopy has provided impressive details on the distribution and form of channel confined selenium, intrachain bond length and conformational information as well as a preliminary insight into quantum size effects in one dimension. From inspection of

Figure 6a, one can determine that only one Se chain is capable of being accommodated in the large channel of mordenite. Occupied mordenite channels could be distinguished from empty channels in high resolution micrographs of Se_n/MOR (Fig. 6d). Here the white bands show white dots for the main and subsidiary channels devoid of selenium, whereas the dark bands show black main channels and white small channels. This confirms that the selenium is indeed incorporated into the large channels of mordenite.

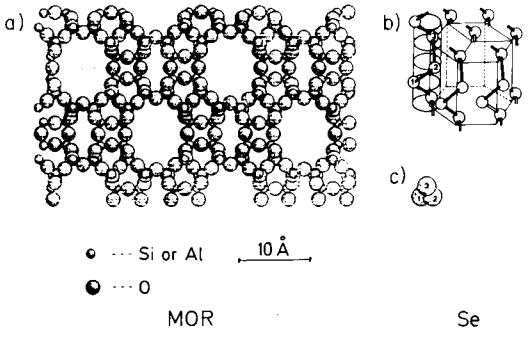

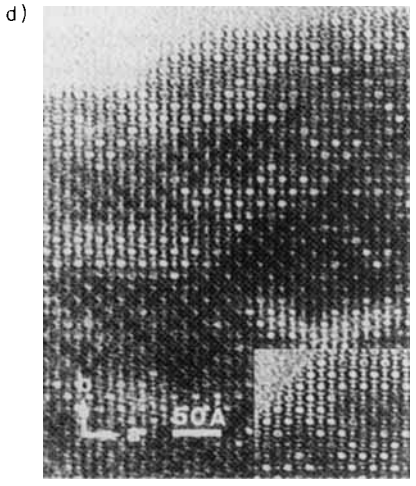

Fig. 6. a) Schematic drawing of the framework structure of mordenite (along [001]). b) The structure of crystalline Se, shown in elevation. c) A projection of the chain of Se along the *c*-axis. d) High-resolution electron micrograph of mordenite into which Se has been inserted. The regions of light contrast are seen to be indistinguishable from mordenite devoid of any guest species. At the regions of dark contrast, caused by uptake of Se the small channels are still empty as indicated by the small white dots [10].

Parise et al.[18] extended the incorporation of selenium chains to other molecular sieves, including zeolites A, X, Y, AlPO-5 and mordenite. Their study showed how the zeolite framework structure can be used to direct the growth of the occluded selenium to its various allotropes. In all samples the band gaps blue-shifted from the respective band gaps of the bulk trigonal and monoclinic forms. While only Se_8 crown rings formed inside zeolite A (band gap close to the value for monoclinic Se: Se_8 rings), helical chains predominated in the other zeolites (band gap-energy close to that for trigonal Se). In the X and Y samples the framework system was occupied by a mixture of selenium allotropes and helical chains. Mordenite and AlPO-5 resulted in the highest degree of order, having single helical chains in the 12-ring channels, with a Se-Se distance (2.34 Å) ca. 2% shorter than in crystalline trigonal Se (2.373 Å).

The particle size dependence of the band gap of semiconductor materials like ZnS, CdS, PbS is now well documented. Their optical properties have been reasonably described by the "electron-hole in a sphere" model of *Brus* and the increase in band gap follows as a result of the 3D spatial confinement of the electron-hole pair. Unlike these isotropic semiconductor particles, selenium is structurally unique in its ability to exist as helical chains and Se_8, Se_7, Se_6 puckered rings, with intraatomic chain and ring bonding being much stronger than inter-chain and inter-ring interactions. It is noteworthy that the theoretical models for size quantization effects in the optical absorption spectra of layered semiconductor colloidal particles involve modifications of the electron-in-a-cubic-box model to account for charge confinement in a rectangular box with an infinite potential barrier, which can be thinned to include the case of a single-layer 2D sheet. Thus it is likely that a different approach will be required to explain the 0.2 eV blue shift observed in the band gap of the intrazeolite Se helical chain, relative to the bulk trigonal phase. A possible contribution to the widened band gaps in the chain form arises from a reduced selenium chain length, and 1D quantum size effects. However, it is difficult to evaluate the role of chain-chain interactions on the 0.2 eV blue shift. A 0.3 eV blue shift observed in intrazeolite Se_8 appears to have its origin in the loss of ring-ring interactions. One should keep in mind that small changes in Se-Se bond lengths, together with alterations in helical pitch and dihedral angle could all contribute to the small differences observed among the optical spectra of intrazeolite selenium and their bulk analogues.

6. Molecular Wires—Conducting Polymers in Zeolites

An intriguing new direction in zeolite science focusses attention on synthetic strategies for the encapsulation of so called molecular wires", composed of "isolated" strands of conducting and semiconducting chain structures like those found in polythiazyl, polypyrrole, and polyaniline, for example, in the unidimensional channel structures of mordenite, L-zeolite and ALPO-5 hosts.

Quite often, the anisotropic electronic, magnetic and optical properties of so-called one-dimensional materials in the bulk solid phase are influenced to some degree by interchain interactions. For example, polythiazyl $(SN)_x$ is a room temperature metallic conductor, which does not un-

dergo a metal insulator Peierls distortion on cooling and, moreover, becomes superconducting at low temperatures. Tunable band filling in 1D solids is often achieved by chemical doping with electron donors or acceptors, or by electrochemical oxidation/reduction. The resulting cation/anion pair interactions are thought to play a role in the properties of the 1D material. Thus "isolated" conducting chains confined to a 1D zeolite channel provide an interesting situation for comparison with "interacting" chains in the bulk.

A recent study by *Bein* and *Enzel*[19] gives an example of the utility of zeolites in such developments. These workers allowed pyrrole (vapor and solution phase) to diffuse into Fe^{III}-containing faujasite (Y) or mordenite (M). The pyrrole polymerized within the channel system where the extraframework Fe^{III} ions served as an oxidant. The polypyrrole chains formed are expected to be 1D molecular conductors. The host pore and channel structure was anticipated to affect the polymer chain length and thus the transport properties of the molecular wires. Using the diagnostic 2.7 eV and 2.0 eV $\pi \rightarrow \pi^*$ absorptions as indicators of the degree of polymerization it was concluded that vapor phase treated $Fe^{III}Y$ contains *shorter* polypyrrole chains than those encapsulated in $Fe^{III}M$. Because of the insolubility of bulk polypyrrole, solvent extraction experiments were incapable of establishing the location (internal vs. external) of the polymerization product. However, indirect evidence provided a case for internal imbibement of the polypyrrole chain. This evidence included a) the inability to form polypyrrole in Na^{I} or Fe^{II} forms of the zeolites compared to the Fe^{III} form, b) the superior UV-visible transmission properties and narrower FT-Raman line widths of zeolite polymerized pyrrole inclusion compared to the bulk form and c) the lesser encapsulation quality of the polymer in the mordenite compared to the Y zeolite host where the former has the smaller free pore volume.

Another material of great interest for the formation of intrazeolitic molecular wires is polyaniline encapsulated in zeolite hosts. Here the possibility exists of obtaining isolated structurally defined chains whose electronic transport behavior can be switched from insulating to conducting by electrochemical oxidation and/or chemical protonation. The selection of acid versus alkali metal ion-exchanged zeolite hosts is therefore crucial in terms of synthetic strategy, details of intrazeolite polymerization, and properties of the resulting encapsulated polymer.

Polyaniline is a novel conducting polymer, salts of which have been synthesized with electrical conductivities up to 10 $\Omega^{-1}\,cm^{-1}$. In contrast to polypyrrole, which contains nitrogens as pendant groups attached to a polyacetylene like backbone, polyaniline exists with amine and imine nitrogen atoms (the relative amounts dependent on the degree of oxidation) occupying bridging positions in the backbone-structure which, furthermore, can be protonated and deprotonated by an appropriate choice of pH.[20]

Key questions are: What is the state of protonation/oxidation when aniline is polymerized and encapsulated in different zeolite host lattices, and, what are the structure-property relationships between the "isolated" polyaniline chains so formed and their connection (if any) to the bulk polyaniline analogues?

In the first study to address such questions concerning isolated polyaniline chains, the host structures examined were the sodium and Brønsted acid forms of zeolite Y and mordenite.[21] Polyaniline (PANI) was synthesized intrazeolitically via the oxidative polymerization of preloaded anilinium ion. Although ca. 30–50% extractable PANI was probably formed on the external surface, supporting evidence was given for the stabilization of polyaniline *inside* the zeolite channel system. The electronic spectrum of the various zeolite samples indicates that both the oxidized insulating (590 nm) and the conductive (800 nm) forms of PANI had been encapsulated. Polymerization appeared to be favored in the larger pore network of zeolite Y in comparison to mordenite as indicated by the red shift of the 800 nm absorption of the former relative to the latter.

Clearly these studies represent only the beginning of a large and fascinating enquiry on the synthesis, characterization and structure-property relationships of "molecular wires" comprised of isolated conducting polymeric chains in zeolite hosts. Future work will undoubtedly focus attention on other synthetic pathways to intrazeolite "molecular wires", such as electropolymerization, as well as host control over polymer chain length, definition of degree of polymerization and the intriguing question of the transport properties of "isolated" conducting chains.

7. Intrazeolite Multicomponent Electron-Transfer Chains

The utilization of zeolites in the assembly of molecular structures is demonstrated in an elegant experiment by *Mallouk* et al.[22] These workers used zeolite Y to form a molecular chain of three redox-active molecules at a reactive SnO_2 electrode surface. This self-assembly reaction overcame the great difficulty of direct synthesis. The SnO_2-covered electrode surface was allowed to react with the cationic silane (Fig. 7 top) to produce a coating a few monolayers thick. A dense single layer of zeolite particles was formed on the surface, linked to the silane coating by Si-O-Si bridges at free silanol groups. By immersing this electrode-zeolite assembly in a solution, anions and cations were incorporated at three specific ion binding sites: 1) a multiply charged anion (e.g. $[Fe(CN)_6]^{4\ominus}$) on the bridging silane; 2) a large cation (e.g. a substitution-inert metal polypyridyl complex) size-excluded on the outer zeolite surface; and 3) a small cation (e.g. cationic metallocene) that can enter the zeolite framework. The resulting structure shown in Figure 7 (bottom) was characterized electrochemically, by optical spectroscopy and by scanning elec-

ADVANCED MATERIALS

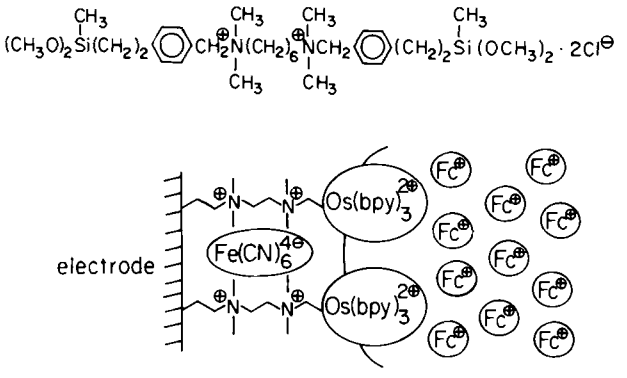

Fig. 7. Top: Cationic silane, used to functionalize the SnO_2 electrode surface before the reaction with zeolite particles. Bottom: Scheme showing the self-assembled redox chains at the zeolite Y-modified electrode. $Fc^{\oplus}$ refers to intrazeolitic cationic metallocenes. The $Os(bpy)_3^{2\oplus}$ complex is size-excluded from the anionic zeolite framework [22].

tron microscopy (SEM). The system functioned as a redox active vectorial chain only when all three components were anchored at their specific sites. Molecular microstructures of this type may serve as models for natural photosynthetic systems.

In another study *Mallouk* et al. have recently achieved long-lived light-induced charge separation in a self-assembling zeolite-based molecular triad.[23] This multicomponent system is composed of a zeolite L or Y surface-bound $RuL_3^{2\ominus}$ sensitizer, an attached $2\,DQ^{2\oplus}$ acceptor (*N,N'*-dialkyl-2,2'-bipyridinium) oriented into the open anionic structure of the zeolite and a secondary acceptor, benzylviologen ($BV^{2\oplus}$), contained within the zeolite framework (Fig. 8). Transient diffuse reflectance and luminescence lifetime measurements on this organized assembly show that intramolecular electron-transfer quenching from $Ru^{2\oplus}$ to the $2\,DQ^{2\oplus}$ moiety occurs within 5 ns or less and that the formation of the $Ru^{3\oplus}$-$BV^{\oplus}$ charge-separated state occurs in about 100 ns; this indicates that electron transfer from

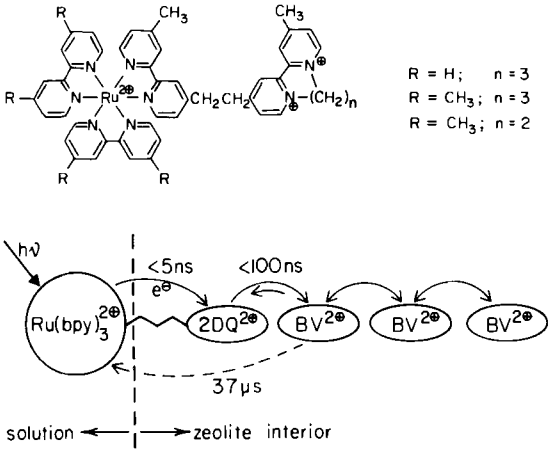

Fig. 8. Possible spatial arrangement of the $RuL_3^{2\oplus}$-$2\,DQ^{2\oplus}$ complex and $BV^{2\oplus}$ at the aqueous solution/zeolite interface. The structure of the $RuL_3^{2\oplus}$-$n\,DQ^{2\oplus}$ complex is also shown [23].

$2\,DQ^{\oplus}$ to $BV^{2\oplus}$ is complete within ≤ 100 ns. Of particular note is the long-lived nature of the $Ru^{3\oplus}$-$BV^{\oplus}$ charge-separated state, which decays via first-order kinetics with a lifetime of 37 ± 5 μs. The quantum yield for its formation is $17 \pm 5\%$.

The kind of spatial arrangement of the molecular triad shown in Figure 8 is considered to provide close contact of $BV^{2\oplus}$ contained in the zeolite with transiently formed $2\,DQ^{\oplus}$. This permits fast and efficient formation of $BV^{\oplus}$. The long lifetime of the charge-separated $Ru^{3\oplus}$-$BV^{\oplus}$ state has been attributed to a favorable spatial separation of $Ru^{3\oplus}$ and $BV^{\oplus}$ and the possibility of isoenergetic electron-exchange along the $BV^{2\oplus}$ chain depicted in Figure 8.

The work of *Mallouk* et al. has relevance to electron-transfer reactions in photosynthetic chains and light-to-chemical energy conversion systems. Of special note is the fact that the zeolite-based triad spatially resembles and behaves like the membrane-bound special pair-pheophytin-quinone triad in the reaction center of photosynthetic bacteria, which has two extremely fast forward electron-transfer steps and a long-lived charge-separated state.

8. Zeolite Electrodes—Zeolite-Modified Electrodes

Zeolites are essentially cationic conductors with the same temperature dependence typically displayed by solid ionic conductors (higher mobility of ions at higher temperature). However, some indications of partial electronic conductivity exist, for example in silver exchanged zeolite A.[24] By appropriate modifications of the zeolite composition the conductivity properties of zeolites can be altered to allow their use as solid electrolytes, membranes in ion-selective electrodes and as host structures for cathode materials in battery systems.[25]

Two types of applications exist for zeolites as part of electrode systems. In zeolite-modified electrodes the zeolite acts as a charge, size and shape selective membrane to impart a chemically specific environment for absorbed molecules at an electrode surface.[26] High product selectivities can be obtained with zeolite-modified electrodes in electrosynthetic reactions.[27] The second type, an ultramicroelectrode utilizes the zeolite framework as a matrix for intrazeolitically generated electrode components. Typically metals or metal oxides serve as electrode microstructures in and/or on the zeolite support, but organometallic or organic components, such as the polypyrrole quantum wires mentioned above can also be utilized. Organic molecular ultramicroelectrodes allow the study of conductivity and electrochemical reactivity on very small scales, as well as electrode processes at shorter times, in restricted environments and unconventional media.[26] They have potential relevance to photosynthetic systems and molecular electronics (e.g. sensors, solid state devices).

The zeolite electrode systems to be briefly described in this section include: a) encapsulated Pt_n clusters; b)

$M(bpy)_3^{2\oplus}/M(CpR)_2^{\oplus}$; c) $EDTA/MV^{2\oplus}/ZnTMPyP^{4\oplus}/Pt_n$; d) $MV^{2\oplus}/CoTMPyP^{4\oplus}$; e) $MnTMPyP^{5\oplus}$; f) composite zeolite electrodes.

An important question in all these systems is that of making electrical contacts. Some commonly used methods include 1) spring loaded contacts or coatings such as silver paint with zeolite pellets; 2) molecular attachments such as in the methylviologen-porphyrin studies described in the previous section; and 3) a method developed by *Pons* et al.[28] that avoids fixed electrical contacts altogether. The latter method consists of applying bipolar electrolytic conditions to dispersions of ultramicroelectrodes using feeder electrodes. The zeolite-supported ultramicroelectrode acts both as a mobile electrode and an electrolyte. A wide range of ultramicroelectrodes can then be accessed. This technique was applied in the study of zeolite encapsulated metal clusters for dispersion electrolyses,[26,29] as outlined below.

In practice one finds that zeolite supported platinum clusters permit dispersion electrolyses under low ionic strength conditions where microelectrodes could not function. Pt_n/zeolite Y has been shown to be a much more effective ultramicroelectrode system than $Pt_n/\gamma\text{-}Al_2O_3$ for aqueous electrolyses.[29] Control experiments showed that, although an increase in the conductivity of aqueous media did ensue from ions exchanged from the virgin zeolite, the higher ohmic background was dwarfed by the electrochemical response obtained in the presence of platinum supported in the zeolite.

Gallezot's procedures for the formation, location and sizing of Pt_n in zeolite Y were employed in the fabrication of the Pt-Y electrodes. After $[Pt(NH_3)_4]^{2\oplus}$ ion-exchange for $Na^{\oplus}$ in Na-Y, the zeolite was dried at 135°C and then heated in flowing oxygen to promote H_2O/NH_3 loss and autoreduction of Pt^{II} to Pt^0 via NH_3. The details of the activation step were crucial in determining the state and distribution of Pt_n within the zeolite microstructure. At 300°C, 6-13 Å Pt_n remained in the supercages while at 600°C, 15-20 Pt_n formed throughout the bulk of the crystal.

Typical results for the two-phase system C_6H_6/H_2O showed markedly enhanced currents at a given voltage for 1% Pt-Y (with mainly internally sited platinum), compared to 1% $Pt\text{-}Al_2O_3$, and essentially zero response for the feeder electrodes alone. The current-voltage responses of different Pt-Y loaded samples for the electrolysis of water showed that the electrolytic effectiveness followed the order: 1% Pt-Y > 5% Pt-Y > 10% Pt-Y = 1% $Pt\text{-}Al_2O_3$. Comparisons between the electrolyte response of Pt-Y samples, implied that the internally confined particles did not contribute to the electrolyses. This was rationalized by the inability to achieve electric fields high enough for bipolar electrolysis to occur on intracrystalline sited platinum particles at the voltages employed. By contrast, externally sited particles could be physically charged at the feeder electrode or via other previously charged supported platinum sites. Similar effects have been experienced for dispersion electrolysis of ferrocene/CH_3CN and a substituted ferrocene/CH_3CN too bulky to enter the Pt-Y sample, thereby supporting the proposal of externally active platinum sites in Pt-Y. In the dispersion electrolysis the zeolite support yielded a more effective material than the alumina. Based on XPS determined platinum particle sizes and associated surface areas these results suggest that the electrode processes may be affected by particle size in the submicron range.

Recently the preparation and electrochemical behavior of simple, self-assembly vectorial electron transport chains on zeolite Y modified SnO_2 electrodes have been described.[27] These involve a Y zeolite which has been ion exchanged with a tris(bipyridyl) metal complex $M(bpy)_3^{2\oplus}$ (M = Ru, Os), and a metallocene cation $M(CpR)_2^{\oplus}$ and $M(Cp)(CpR)^{\oplus}$ (M = Co, Fe; Cp = η^5-C_5H_5 and R = H, CH_3, NH_2, CO_2CH_3, $CH_2N(CH_3)_2$). Matching of the potentials of externally sited $M(bpy)_3^{2\oplus}$ and intrazeolite $M(CpR)_2^{\oplus}$ ensures facile redox reactions, an order of magnitude enhanced over the situation when $M(bpy)_3^{2\oplus}$ is absent from the system. Rapid electron-transfer cross reactions between the two complexes are proposed to explain this behavior.

Electrodes were prepared from conductive SnO_2 coated glass squares contacted to copper wire via colloidal silver paint. The electrode was dipped into a suspension containing the ion-exchanged zeolite and polystyrene in THF, and was allowed to dry in air. Scanning transmission electron microscopy and electron diffraction (STEM) experiments on freshly cleaved electrodes showed a film thickness of about 60 μm with most of the polystyrene forming a porous layer at the outer surface of the film. The metal guest was located in the ca. 1 μm zeolite particles which formed a porous compact layer tightly adhering to the SnO_2 substrate.

Reduction and oxidation peaks of the surface bound couple $Ru(bpy)_3^{2\oplus/1\oplus}/ZY/SnO_2$ occurred at −0.76 and −0.55 V vs. the saturated calomel electrode (SCE). It is interesting that the $E_{1/2}$ of this couple ($E_0 = -0.66$ V vs. SCE) was shifted about 600 mV positive of its value in polar organic solvents (−1.24 V vs. SCE), pointing to the stabilizing effect of adsorption of $Ru(bpy)_3^{1\oplus}$ relative to $Ru(bpy)_3^{2\oplus}$ on the zeolite. The quantity of charge passed in the $Ru(bpy)_3^{2\oplus}$ reduction wave indicated that only the surface $Ru(bpy)_3^{2\oplus}$ contacting the SnO_2 electrode was electrochemically accessible. In the case of a $Co(CpCH_3)_2^{1\oplus}/ZY/SnO_2$ electrode only a small fraction of the intrazeolite $Co(CpCH_3)_2^{\oplus}$ was reduced or oxidized. The $E_{1/2}$ of $Co(CpCH_3)_2^{1\oplus/0}$ also shifted to a more positive value (−0.66 V vs. SCE) compared to its solution phase value (−1.10 V vs. SCE). A tenfold increase in the height of the cathodic wave for an $Ru(bpy)_3^{2\oplus}/Co(CpCH_3)_2^{1\oplus}/ZY/SnO_2$ electrode was observed compared to the case when surface bound $Ru(bpy)_3^{2\oplus}$ was absent. Similar current enhancements were obtained for a number of substituted

ADVANCED MATERIALS

$Co(CpR)_2^{1\oplus}$ species provided that the respective $E_{1/2}$ was positive or coincident with the $Ru(bpy)_3^{2\oplus}$ wave. The mechanism shown in Figure 9a was proposed to rationalize the observation of current enhancement, where the large cathodic wave represents the reduction of bulk $Co(CpR)_2^{1\oplus}$ mediated by surface adsorbed $Ru(bpy)_3^{2\oplus}$. The observed enhanced anodic wave was ascribed to the reverse electrocatalytic reaction shown in Figure 9b. The key finding of this study is that rapid vectorial electron transfer from the electrode to the bulk materials occurs almost entirely through the $M(bpy)_3^{2\oplus}$ complex.

a) *Cathodic process:*

$$Ru(bpy)_3^{2\oplus}(surf.) + e^{\ominus}(electrode) \longrightarrow Ru(bpy)_3^{\oplus}(surf.)$$
$$\uparrow$$
$$Ru(bpy)_3^{2\oplus}(surf.) + Co(CpCH_3)_2^{0}(bulk) \longleftarrow Co(CpCH_3)_2^{\oplus}(bulk)$$

b) *Anodic process:*

$$Ru(bpy)_3^{2\oplus}(surf.) + Co(CpCH_3)_2^{0}(bulk) \longrightarrow Co(CpCH_3)_2^{\oplus}(bulk)$$
$$\uparrow \qquad\qquad\qquad\qquad +$$
$$Ru(bpy)_3^{2\oplus}(surf.) + e^{\ominus}(electrode) \longleftarrow Ru(bpy)_3^{\oplus}(surf.)$$

Fig. 9. Proposed mechanisms for the cathodic and anodic reactions at a $Co(CpCH_3)_2^{1\oplus}/ZY/SnO_2$ electrode [27].

Experiments of this kind stimulated research on more sophisticated intrazeolite molecular electron transport chains composed of porphyrins and viologens. Two fascinating new systems will be referred to, one involving photochemical H_2 evolution via singlet-state electron-transfer quenching of zinc tetra(*N*-methyl-4-pyridyl) porphyrin cations ($ZnTMPy^{4\oplus}$) using internally platinized zeolite L particles (Fig. 10a),[30] the other involving current rectification and electron trapping by surface bound monomolecular metalloporphyrin layers on zeolite Y containing intrazeolite viologens (Fig. 10b).[31]

The first zeolite electrode concerns a metalloporphyrin-based electron-transport chain which self-assembles by virtue of ion-exchange and steric interactions with a zeolite L particle. The microstructure imposed by the zeolite permits $ZnTMPyP^{4\oplus}$ to be held in sufficient proximity to a $MV^{2\oplus}$ cation so that singlet-state electron-transfer quenching occurs on the sub-nanosecond time scale. With $EDTA^{2\ominus}$ added as a sacrificial electron donor, H_2 is evolved from water under illumination with visible light at the internal platinized zeolite L-containing $ZnTMPyP^{4\oplus}$ and $MV^{2\oplus}$. Figure 10a displays the fabrication and operating details of this compartmentalized photochemical system. The linear channels which run through zeolite L and bind $MV^{2\oplus}$ are shown as idealized hexagonal prisms. The zeolite outer surface strongly binds the $ZnTMPyP^{4\oplus}$ cation as it is size excluded from the bulk. When a more sterically hindered porphyrin replaces $ZnTMPyP^{4\oplus}$, a system results which is inactive for both H_2 evolution and singlet state quenching by $MV^{2\oplus}$. These observations are rationalized in terms of closely assembled and organized triads of molecules

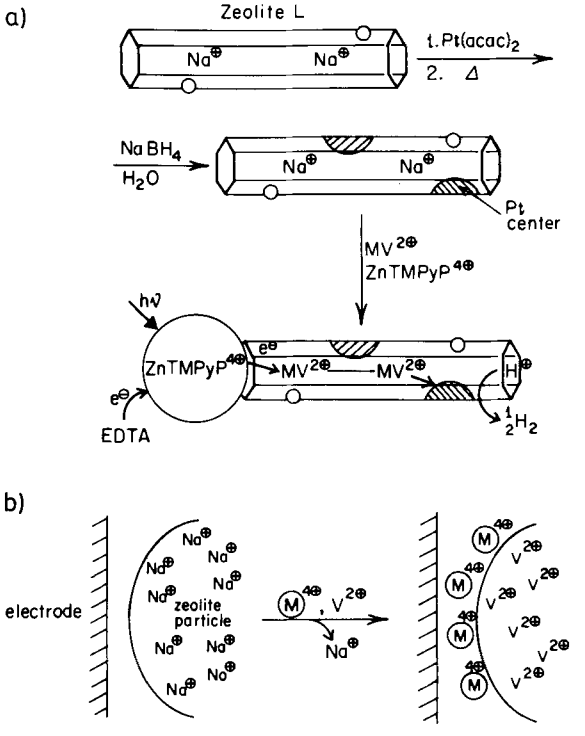

Fig. 10. a) Preparation and operation of the compartmentalized photochemical system, composed of platinized zeolite L containing $ZnTMPyP^{4\oplus}$ and $MV^{2\oplus}$ [30]. b) Preparation of metalloporphyrin/viologen($V^{2\oplus}$)-exchanged zeolite Y particles and zeolite-modified electrodes [31].

$EDTA^{2\ominus}$, $ZnTMPyP^{4\oplus}$, $MV^{2\oplus}$ located at the zeolite/solution interface.

This elegant study demonstrates that molecular level organization of electron donor, metalloporphyrin and quencher in zeolite L is feasible. Such integrated, highly ordered systems can sustain photochemical production of H_2 from water via singlet state electron transfer quenching of the porphyrin molecule. An attractive feature of the system is its self-assembly by ion-exchange from simple commercially available components. Considerable scope clearly exists for maximizing quantum yields for electron-hole separation through the clever design of more complex interfacial assemblies.

Li et al.[31] exchanged zeolite Y with viologen cations which diffused into the bulk and attached monolayers of larger cobalt or zinc porphyrin cations to the outer surface of the zeolite. The porphyrin molecules sealed the zeolite against rapid exchange of viologen molecules and facilitated the electron transfer between the encapsulated viologen ions and the surroundings of the microstructure. The porphyrin tends to remain attached to the zeolite surface because its ionic charge is high enough to avoid exchange with the ionic species of the solution, even in reduced forms of complexed metal.[32]

Another zeolite electrode system of this type was fabricated using $Mn^{III}TMPyP^{5\oplus}$ fixed onto the outer surface of zeolite Y (ZY) in contact with a controlled potential metal-

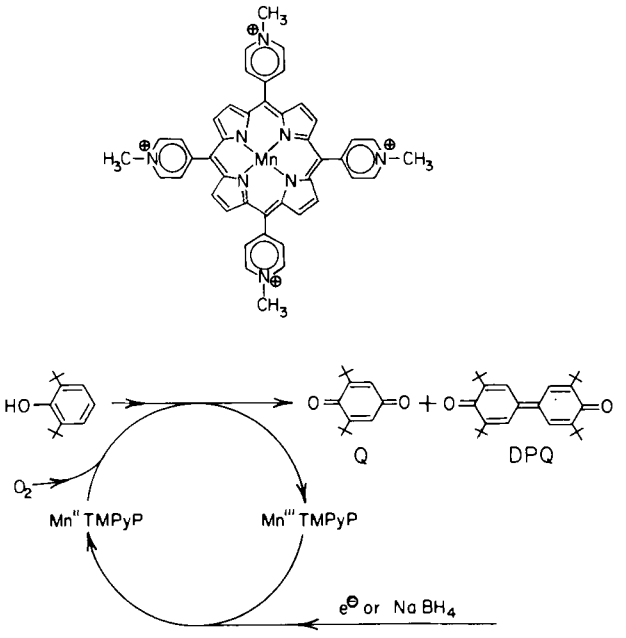

Fig. 11. Catalytic oxidation of 2,6-di-*tert*-butylphenol using a controlled potential metallic electrode (Pt grid) composed of $Mn^{III}TMPyP^{5\oplus}$ fixed onto the outer surface of zeolite Y [32].

lic electrode (Pt grid).[32] The test reaction was the oxidation of 2,6-di-*tert*-butylphenol to produce 2,6-di-*tert*-butyl-*p*-benzoquinone (Q) and diphenoquinone (DPQ). The overall catalytic process is summarized in Figure 11, where the catalytic species is $Mn^{II}TMPyP^{4\oplus}$. The study proves that $Mn^{III}TMPyP^{5\oplus}/ZY$ participates in the heterogeneous catalyzed O_2 oxidation of di-*tert*-butylphenol with quantitative conversion of the phenol to the quinone products and electrochemical regeneration of the catalyst.

The response of zeolite electrodes can be optimized by preparing a composite electrode with carbon paste. For example, *Creasy* and *Shaw*[33] constructed electrodes of methyl viologen exchanged zeolites Y and A mixed with carbon paste for the electroreduction of oxygen. The results showed that the electroreduction of oxygen by methyl viologen proceeded more efficiently upon incorporation of zeolite Y into a carbon paste electrode and that efficient mediation required the zeolite to be in close proximity to the conducting carbon particles. An optimum current was obtained when the zeolite was saturated with methylviologen.

Other zeolite composite electrodes have been formed by codepositing zeolites with organic salts or polystyrene, mixing them with conductive carbon powder or pressing them into pellets coated with doped tin oxide.[34]

9. Zeolite Solid State Batteries

In the context of advanced zeolite materials science and battery research, it is especially humbling to learn that solid state, multiple-layer zeolite batteries, having excellent high temperature (500°C) and low temperature (−78°C) operating characteristics, were developed by *Freeman* as early as 1965.[35]

The feasibility of fabricating a battery utilizing zeolite materials relates to the fact that zeolites are fairly good solid state ionic conductors with relatively small activation energies for conduction (e.g., dehydrated NaX, $\sigma(Na, 300°C) = 10^{-4}$ to $10^{-5}\ \Omega^{-1}\ cm^{-1}$). Experimentally, two types of ion motion in zeolites have been detected: a) cation jumps from site to site, b) ionic relaxation or restricted local motions of cations. These phenomena in A, X, and Y zeolites are believed to be due to cation mobility in supercages and sodalite cages. The non-monotonic ionic radius dependence of the activation energies for conduction of alkaline metal cations in faujasite has been explained in terms of a model involving coulombic interactions of the cation with the lattice and a repulsive term between cations. Some illustrative data are given in Table 3.[36]

Table 3. Activation energies [kJ mol^{-1}] for cation conduction in faujasite.

Si/Al	1.25	1.7	2.5	2.9
$Li^{\oplus}$	303	—	378	—
$Na^{\oplus}$	219	231	310	332
$K^{\oplus}$	229	226	230	271
$Rb^{\oplus}$	282	282	282	295
$Cs^{\oplus}$	232	243	—	—

Thus the activation energies tend to be larger for small cations and higher Si/Al ratios. Intercation repulsion effects appear to be responsible for the deviation of $Rb^{\oplus}$ and $Cs^{\oplus}$ from this scheme as well as the unexpected Si/Al ordering scheme. When polyvalent cations are exchanged for $Na^{\oplus}$, the activation energy for $Na^{\oplus}$ migration in the supercages, compared to the parent $Na^{\oplus}$ form decreases significantly as seen from Table 4.[36] At low $Ca^{2\oplus}$ loadings, occupancy of sodalite cages with the divalent cation is favored. Thus charge density is localized more in the sodalite cages, resulting in a decreased activation energy for $Na^{\oplus}$ migration in the supercages.

Table 4. Activation energies [kJ mol^{-1}] for cation conduction in faujasite.

Si/Al	1.25		2.5
$Ca_{42}Na_2$	247	$Ca_{26}Na_3$	172
$Ca_{40}Na_6$	192	$Ca_{22}Na_9$	163
$Ca_{35}Na_{16}$	167	$Ca_{20}Na_{15}$	180

Summarizing a large amount of conductivity data, a picture has been advanced for the motion of exchangeable cations in zeolites. It is based on the concept of highly correlated cation jumps and the idea of local cation jumps in, for example, the sodalite cages, usually from AC, DC conductivity and NMR relaxation time measurements.

With the above background material on ionic conduction of extraframework cations in zeolites, let us briefly

ADVANCED MATERIALS

turn our attention to *Freeman*'s pioneering studies of zeolite batteries. Using the original notation of *Freeman* to describe a zeolite multiple layer cell composition:

$|Au|Cu^{II}X|NaX|Zn|$

one speaks of a gold catholyte contact, a copper-exchanged zeolite X catholyte, a sodium zeolite X separator and a zinc anode. The operation of the cell appears to be zinc oxidation at the anode with the liberation of electrons and concomitant reduction of Cu^{II}. This must be accompanied by the necessary ionic charge transfer of Zn^{II} liberated from the anode passing through the NaX separator lattice, to find a cation vacancy probably in the $Cu^{II}X$ lattice. Open circuit voltages for cells fabricated by pressed pellet techniques were found to be surprisingly reproducible and fell in the range 1.36–1.40 V with $Ag^{I}X$ as zeolite catholyte and calcium exchanged zeolite A (CaA) as separator, or 1.17–1.25 V with a $Hg^{II}X$ catholyte. The $|Au|Hg^{II}X|NaX|Zn|$ cell is particularly outstanding in that an appreciable current could be drawn with only a 23% drop in voltage as the load was applied.

Since most zeolites are thermally stable to at least 750°C, zeolite cells are operable at unusually high temperatures, providing the contacts, electrodes, and intrazeolite metals are stable. In $Au|Cu^{II}X|NaX|Zn|$ an exponential increase in current with temperature is found over the range from 260°C (3×10^{-7} A output current) to 500°C (2.8×10^{-5} A).

The $|Au|Ag^{I}X|CaA|Mg|$ cells with magnesium anodes displayed the highest open circuit voltages obtained from single zeolite cells (1.95–2.10 V, for four different cells). It is remarkable that a $|Au|Hg^{II}X|CaA|Zn|$ cell could be operated at −78°C with an open circuit voltage of about 1.0 V compared to 1.1 V at room temperature.

In a more recent vein, *Andersen* et al.[37] have used AC conductivity measurements on $NH_4^{\oplus}$ and $H_3O^{\oplus}$ zeolites A, X, Y and have established that $NH_4^{\oplus}$ and $H_3O^{\oplus}$ cations are mobile with conductivities dependent on the degree of hydration of the zeolite. Cell reactions have been developed for these zeolites which exploit the mobilities of the proton and ammonium ions. Cells were constructed from porous platinum blocking electrodes deposited onto pressed zeolite wafers as illustrated below:

$H_2|Pt|H_3O^{\oplus}Z|Pt|H_2$

Here the half reactions at the porous platinum electrodes involve:

$$1/2\,H_2 \longrightarrow H^{\oplus} + e^{\ominus} \quad \text{anode}$$

$$H^{\oplus} + e^{\ominus} \longrightarrow 1/2\,H_2 \quad \text{cathode}$$

where the proton conductivity involves $H_3O^{\oplus}$ transfer across the solid zeolite electrolyte layer. An interesting extension of this idea involves an NH_4Z solid state electrolyte cell:

$H_2|Pt|NH_4^{\oplus}Z^{\ominus}|Pt|H_2$

where in a similar arrangement $NH_4^{\oplus}$ is gradually replaced by $H_3O^{\oplus}$ with NH_3 evolved at the cathode according to the following cell reactions:

$$H_2O + 1/2\,H_2 \longrightarrow H_3O^{\oplus} + e^{\ominus} \quad \text{anode}$$

$$H_3O^{\oplus} + NH_4^{\oplus}Z \longrightarrow H_3O^{\oplus}Z + NH_4^{\oplus} \quad \text{zeolite electrolyte}$$

$$NH_4^{\oplus} + e^{\ominus} \longrightarrow NH_3 + 1/2\,H_2 \quad \text{cathode}$$

These results are quite fascinating and clearly have ramifications in advanced battery and fuel cell applications, as well as in electrochromic zeolite and molecular size/shape selective ionic-conductivity sensor elements.

Another interesting solid state zeolite cell involves the concept of utilizing dehydrated zeolite crystals as host structures for liquid and volatile electrochemically active species. *Coetzer* et al.[38] have employed this idea to investigate the performance of zeolite/iodine and zeolite/sulfur cathodes in solid state cells. For example, dehydrated sodium exchanged zeolite A (NaA) impregnated with I_2 has been used as a cathode material in a silver/I_2 solid state cell as shown in Figure 12.

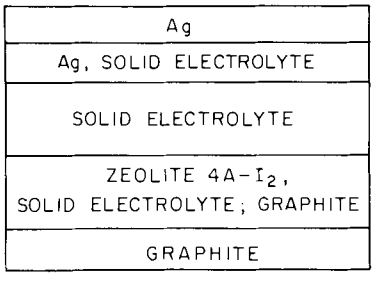

Fig. 12. A diagrammatic sketch of a Ag/zeolite 4A-I_2 cell [38].

Two quaternary amine iodide/AgI solid electrolytes, namely $Ag_{44}I_{53}(C_{11}H_{30}N_3)_3$ and $Ag_{21}I_{25}(C_9H_{24}N_2)_2$ having room temperature ionic conductivities of ca. $3 \times 10^{-2}\ \Omega^{-1}\ cm^{-1}$ are used in these cells instead of well known $Ag^{\oplus}$ conductors like $RbAg_4I_5$, as the latter is electrolytically unstable in the presence of elemental iodine. Thus it is advantageous to complex the iodine in the cathode in some way at reduced activity, as found in RbI_3, Me_4NI_5 and Me_4NI_9. The NaA/I_2 cathode is another way of achieving the goal of controlled iodine release for the cell reaction $2Ag + I_2 \rightarrow 2AgI$.

The NaA/I_2 complex used contained 38.9 wt% I_2 giving the formula $Na_{12}Al_{12}Si_{12}O_{48} \cdot 4.3\,I_2$ for the zeolite/I_2 storage cathode. A multilayer, 20 mm diameter cell construction was employed. Anode and cathode components contained finely ground electrolyte material to enhance elec-

trode-electrolyte interfacial contacts and disc binding qualities, while the cathode was mixed with finely divided graphite to enhance the electronic conductivity as the zeolites are electronic insulators.

The formation of resistive AgI ($\sigma_{25°C} \approx 10^{-4}\ \Omega^{-1}\ cm^{-1}$) as the only discharge product in the $NaA/I_2/Ag$ cell caused the internal resistance to rise and the load voltage to drop accordingly with time. This necessitates the use of relatively thin cathodes for this type of cell (cf. the Li/2-polyvinylpyridine-I_2 heart pacemaker[39]).

In summary, these results illustrate the intriguing possibility of immobilizing volatile electrochemically active species in zeolites for use as cathodes in ambient temperature cells. The immense flexibility in the choice of a zeolite host offers great opportunities for optimizing an electroactive guest molecule. One might remark on concluding this section, that it is rather surprising that the literature on zeolite batteries has been quite sparse since *Freeman*'s early pioneering work. It is expected that this situation will change rapidly as research in zeolite materials science gathers momentum in the late 1980's.

10. Optozeolite Chemical Sensors

A sensor can be defined as a small device that converts any microchange of temperature, pressure, concentration or other property into a detectable signal. The success of a chemical sensor is determined by its sensitivity and reproducible performance. The sensing element is expected to incorporate at least the following attributes: selectivity and site reversibility with respect to guest binding, fast response, small size, ruggedness, low cost, and the potential for facile integration into an automated system. With respect to sensor architecture most devices today employ a union between a selective chemireceptor and a transducer which is capable of translating the resulting physicochemical perturbation into a usable signal. Gas-sensitive metal gate semiconductor devices, chemically sensitive field effect transistors, Schottky diodes, chemiresistors and surface acoustic wave sensors represent just a few of the emerging technologies with promise in the chemical sensor field.

The concept of using zeolites as size and shape selective chemical sensors was at the basis of our research efforts to elicit from such materials an optical response such as intensity and lifetime modification due to intrusion of an adsorbate into the pore system of a zeolite. It is noteworthy that the recent patent literature mentions zeolites in applications ranging from moisture sensing,[40] oxygen monitoring,[41] and carbon monoxide detection[42] to the selective detection of ethylene, ethane and propylene.[43]

Luminescent centers housed in various zeolites were selected mainly from $Eu^{3\oplus}$, $Mn^{2\oplus}$ and $Ag^{\oplus}$ which have an extensive photochemical/photophysical solid-state literature for a range of hosts. These include single crystals, glasses, layered materials and oxide supports. Although the optical absorption and luminescence properties of certain intrazeolite metal guests are quite well understood, little is known about their excited state lifetime properties. Even less information is available on the response of these properties to specific molecule absorption and luminescence quenching in the time domain. An attractive feature of intrazeolite luminescent metal probes (ILMP's) is that one can fine-tune their optical characteristics over useful ranges of frequency and, as has been discovered recently, in time. Parameters that can be varied include the zeolite type, co-cations, Si/Al ratio and loading of the ILMP. A useful example of loading and co-cation effects stems from luminescence lifetime data obtained from the study of

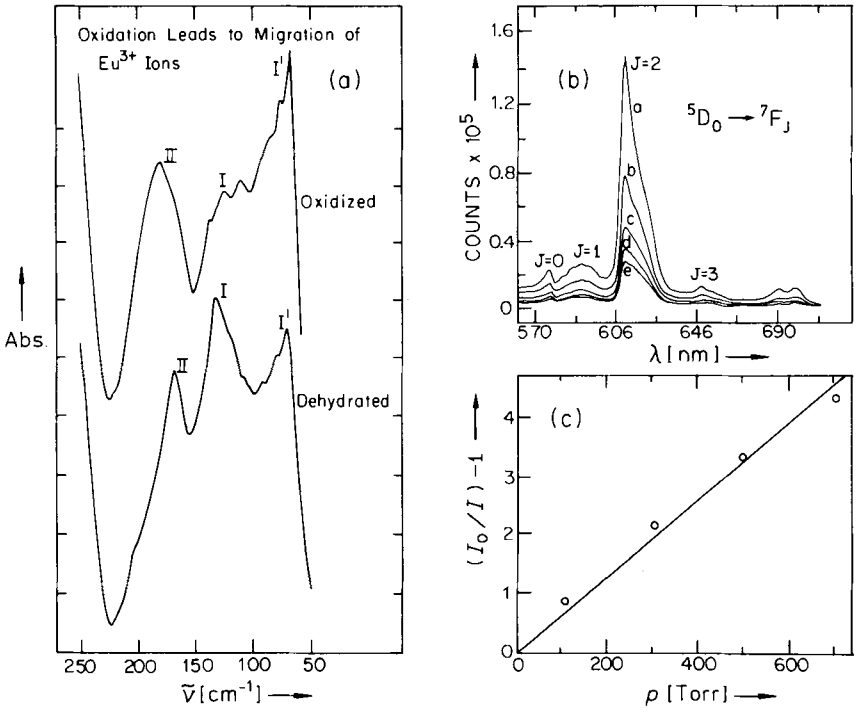

Fig. 13. a) Far infrared spectra of $Eu^{3\oplus}Y$. b) The quenching of $Eu^{3\oplus}$ luminescence at various oxygen pressures: a: vacuum, b: 105 Torr, c: 500 Torr, d: 700 Torr, e: 760 Torr. c) Stern-Volmer plot for the $J=2$ luminescence quenching depicted in b) [44].

silver faujasites.[44a,b] The observed long-lived emissions have been associated with a spin-forbidden phosphorescence of intrazeolite $Ag_2^{\oplus}$.

The impetus for the study of $Eu^{3\oplus}$-ZY was the intrinsic very bright fluorescence of $Eu^{3\oplus}$ and the well understood luminescence spectroscopy in other solids. $Eu^{3\oplus}$ cation site locations within zeolite Y were established by far infrared spectroscopy that conveniently pinpoints cation translatory modes (Fig. 13a). The fluorescence intensity of $Eu^{3\oplus}$ was quenched upon admission of oxygen (Fig. 13b). A study of the O_2-concentration effect showed that the quenching kinetics were Stern–Volmer in nature (Fig. 13c). The lifetime decays of $Eu^{3\oplus}$-ZY also showed sensitivity to oxygen (Fig. 14). These O_2 quenching effects were found to be completely reversible at room temperature. These results demonstrate that the concept of a time-domain zeolite sensor is valid.

The sensing of NH_3 by $Eu^{3\oplus}$-ZY is noteworthy (Fig. 14b). The response was rather different to that given by O_2. While the $Eu^{3\oplus}$ $J=2$ transition decreased in intensity the $J=0$ transition was enhanced as the pressure of NH_3 was increased. The behavior was reversible upon heating the zeolite to 200°C. This is indeed a unique response. None of the adsorbates screened so far (H_2, N_2, CO, C_2H_4, O_2) produced this signature. The unusual NH_3 effect is believed to originate from a dramatic change in symmetry at the $Eu^{3\oplus}$ ion, possibly due to complexation of $Eu^{3\oplus}$ by NH_3 or the presence of $NH_4^{\oplus}$ ions formed by the interaction of NH_3 with the lattice hydroxy groups, the latter being formed from the hydrolysis of H_2O by $Eu^{3\oplus}$.[44a,b]

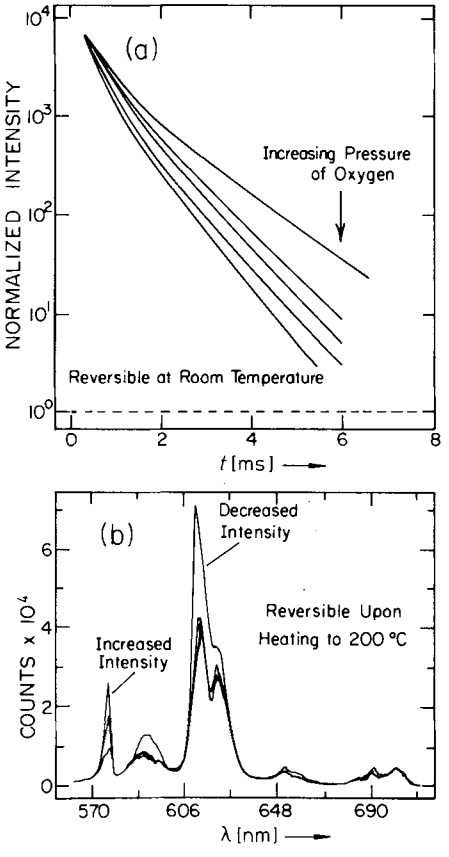

Fig. 14. a) Lifetime quenching of $Eu^{3\oplus}$-ZY luminescence by oxygen. b) The quenching of $Eu^{3\oplus}$ luminescence in zeolite X by ammonia [44].

The new generation MnAPO and MnAPSO molecular sieves provide a unique opportunity for studying the photophysical behavior of a luminescent $Mn^{2\oplus}$ framework probe. Most detailed results have been obtained so far with the MnAPSO-31 and 44 template-containing and template-free materials.[44c] Detailed EPR, steady state and time resolved optical reflectance/emission spectroscopic studies of these materials have yielded evidence for magnetic and electric dipole-coupled $Mn^{2\oplus}$ framework centers, some sites experiencing detectable interactions with neighboring template molecules.[44c]

Laser induced fluorescence studies aimed at exploring specific adsorbate quenching effects in template free MnAPSO-44 have been performed. N_2O, CO, N_2 and O_2 show reversible intensity quenching responses. Whether these are dynamic and/or static and molecule specific has yet to be quantified. It is notable that Ar, CH_4, C_3H_6 and CH_3COOCH_3 display no intensity quenching effects under similar conditions while quenching with NH_3 is irreversible. These results are encouraging as they suggest that framework metal luminescent centers might be susceptible to selective adsorbate quenching. Clearly these early studies represent just a modest beginning. Much fascinating work remains to be done in the search for a molecule size/shape discriminating optozeolite chemical sensor.

11. Tunable Non-Linear Optical Zeolites

The development of new non-linear optical (NLO) materials, which allow frequency multiplication and mixing of UV-VIS-IR radiation for laser and electrooptics applications (optical processing/computing, image analysis, switches, modulators) has recently been extended into the world of zeolites. *Cox* et al.[45] have given the first report of a non-linear optical material, fabricated by the confinement of an organic guest in an acentric zeolite host with a one-dimensional channel structure.

NLO effects are usually obtained by the polarization of a medium by an incident electric field:

$$P = \chi_1 E + \chi_2 E^2 + \chi_3 E^3 + \cdots$$

χ_1 = first order susceptibility tensor (linear optical properties, refraction, absorption); χ_2 = second order susceptibility tensor (zero for centrosymmetrical materials; non-zero values yield frequency doubling, frequency mixing effects); χ_3 = third order susceptibility tensor (non-zero for all materials, provides access to the Kerr effect, self focussing, degenerate four wave mixing, third harmonic generation).

The connection of electric susceptibilities to NLO effects derives from the polarization induced by an oscillating dipole which radiates energy. The electric field associated with the radiating dipole is proportional to the polarization:

$$E_{rad} \propto P(\omega) \quad \text{or} \quad P(2\omega) \quad \text{or} \quad P(3\omega)$$

Therefore the intensity of the radiating signal is given by

$$I \propto |E_{rad}|^2$$

and for second harmonic generation

$$I(2\omega) \propto |\chi_2|^2 I^2(\omega).$$

In order to relate microscopic to macroscopic susceptibilities one considers first the molecular response to electric fields:

$$\mu = \mu_0 + \alpha E + \beta E^2 + \gamma E^2 + \cdots$$

μ_0 = permanent GS dipole moment, α = linear polarizability (2nd rank tensor, proportional to χ_1), β = second order polarizability (3rd rank tensor, proportional to χ_2), γ = third order polarizability (4th rank tensor, proportional to χ_3).

Each component molecule of a material acts as a source of non-linear polarization and so the macroscopic response is the sum of the macroscopic responses averaged over all orientations. For second harmonic generation (SHG), χ_2 must be non-zero. To achieve this objective it is mandatory that all molecular dipoles point in the same direction on average, that is:

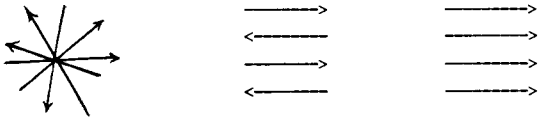

Random	Alignment	Orientation
$\chi_2 = 0$	$\chi_2 = 0$	$\chi_2 \neq 0$

It is difficult to orient small molecules by electric or magnetic fields, because of their small dipole moments and magnetic susceptibilities. Thus it is clearly beneficial to incorporate such molecules into larger host structures to enhance orientation and alignment in addition to other properties such as mechanical stability and processibility etc. The non-centrosymmetric structural features required for SHG may be imposed on a guest species by an acentric zeolite host. In some cases synergistic sorbate-host interactions between two centric species yield a non-centrosymmetric product with very different NLO properties from either guest or host. *Cox* et al.[45] have incorporated *p*-nitroaniline (NA) and 2-methyl-*p*-nitroaniline (MNA) in zeolites Y, Omega, Mordenite and AlPO-5 in order to study changes in SHG. Note that NA has a large hyperpolarizability β but crystallizes centrosymmetrically giving $\chi_2 = 0$. To overcome the problem of relative orientation of molecules in a solid various kinds of molecular engineering approaches have been investigated, such as simple chemical modification to induce non-centrosymmetric crystallization or inclusion tuning of the organic guest by encapsulation into an acentric inorganic or organic host lattice.

NA in the centrosymmetric molecular sieves zeolite Y, Omega and Mordenite showed no SHG. For the case of NA in the acentric zeolite ALPO-5, a loading dependence of the SHG signal was observed with a maximum SHG of 630 relative to quartz at 13 wt% NA loading when all the pores were filled (Fig. 15) a magnitude *ten* times larger

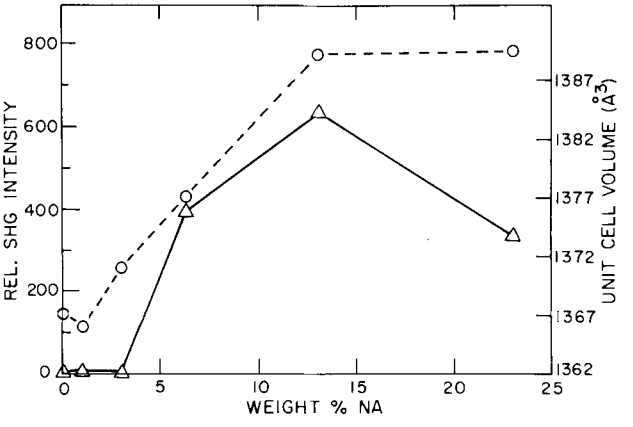

Fig. 15. *p*-Nitroaniline (NA) in ALPO-5. Loading level (weight % NA) versus SHG intensity relative to quartz (solid line) and unit cell volume in Å^3 (dashed line) [45].

than that of any previously reported organic or inorganic inclusion complex. The observation of a maximum SHG at full loading implies encapsulation of NA within the pores of the ALPO-5 molecular sieve. MNA, which has a SHG by itself, loses its SHG upon inclusion in ALPO-5. The authors attributed subtle steric, symmetry and host-guest interaction effects to the ability of ALPO-5 to switch the SHG of NA on and that of MNA off. Future work concerning SHG in molecular sieves will focus attention on the effects of loading levels, other acentric hosts, host-guest interactions, and the nature of the guests.

12. Zeolite Membranes and Thin Films

In this section, a brief description will be presented of the recent development of a new generation of zeolite composite films and well-defined inorganic membrane structures that offer controlled porosity in the 10 Å range. The ultimate goal is to employ these microstructures as

"molecular sieve" elements in chemical sensors, so that only those molecules that are able to pass through the membrane are detected at the sensor surface. The methodology employed to create such a molecule size/shape discriminating inorganic membrane structure involves the incorporation of zeolite crystals into a glass or ceramic matrix. The key objective here is to allow only passage of specific molecules through the zeolite channels while the matrix support remains impermeable.

Synthesis of the inorganic matrix derives from well established sol-gel processing technology based on the controlled hydrolysis of tetraethylorthosilicate (TEO), usually in an alcoholic solvent:

$$Si(OEt)_4 + 4H_2O \xrightarrow[\text{base}]{\text{acid or}} Si(OH)_4 + 4EtOH$$

$$n\,Si(OH)_4 \longrightarrow (SiO_2)_n + 2n\,H_2O$$

Depending on the conditions employed (pH, concentrations, temperature, solvent, etc.) condensation and polymerization of silicate species via Si-O-Si bonds can be biased towards either weakly branched "fractal" structures and microporous gels, or compact, fully polymerized colloidal particles and macroporous gels. Acid hydrolysis leads to the former, while base hydrolysis favors the latter. Incorporation of zeolite microcrystals into the sol-gel process followed by viscous sintering can provide a microcomposite thin film, composed of an impermeable silica matrix with "molecular sieving" capabilities determined by the channel architecture of the embedded zeolite.

One step in the development of thin films is the functionalization of the zeolite surface to improve the adherence properties of the zeolite on a substrate material or to use the zeolite itself as a substrate. *Bein* et al.[46] have addressed this question by studying the reactions of mono- and polyfunctional silanes (functional groups OR, Cl, NR_2, H) with zeolite Y surfaces. Although these workers were mainly interested in the possibility of anchoring molecules to the *internal* surface of zeolite pore systems, their conclusions apply similarly to the external surfaces. At moderate reaction temperatures the functional groups at the silane were lost to form bridges to the zeolite framework. As the reaction continued, Si-C bonds were broken at elevated temperatures and more highly substituted siloxane species were anchored to the zeolite framework. As expected, bridged hydroxy groups were found to be far more reactive than terminal hydroxy groups.

Early zeolite membrane experiments by *Bein* et al.[47] focussed attention on silica embedded faujasite and ZSM-5 zeolites. SEM studies revealed a fairly homogeneous dispersion of zeolite crystals in the membrane. Protrusion of single layers of zeolite crystals out of the amorphous matrix made them accessible to probe molecules adsorbing from the gas phase. This feature of these membranes is vital for sensor coatings.

The central issue of molecular access to the membrane-embedded zeolite crystals was addressed by using a surface acoustic wave device in selective adsorption experiments and mid-IR spectroscopy. A thin film of the membrane on a quartz crystal microbalance showed that in the absence of zeolite crystals, acid-catalyzed gel based films did not adsorb even nitrogen. However, gas uptake was observed when the zeolite was incorporated into the silica membrane.

In the mid-IR experiments, the Brønsted acid protons (hydroxy groups) located on the external surface of the zeolite crystals (3720-3750 cm^{-1}) were readily distinguished from internally located zeolite structural hydroxy groups (3640-3540 cm^{-1}). The gel-derived surface OH groups were characterized in the absence of zeolite by broad, weak IR bands with a sharp onset at 3750 cm^{-1} down to ca. 3200 cm^{-1}.

The key experiment involved the behavior of these differently located hydroxy groups to the adsorption of probe organic molecules whose reaction or interaction with hydroxy groups was determined by size/shape (kinetic diameter) and chemical considerations (pyridine, 5.9 Å; $(C_4H_9)_3N$, 8.1 Å; 2,2,4-trimethylpentane, 6.2 Å; NH_3, 2.6 Å; $(C_4F_9)_3N$, 10.2 Å). The results of these size/shape selective adsorption/reaction experiments provided fairly convincing evidence that, in most membranes studied, the zeolites were completely accessible from the gas phase. The membranes excluded molecules which were larger than the pore openings of the zeolite embedded in the composite. This type of microcomposite membrane is envisaged to offer great opportunities in the development of size/shape discriminating chemical sensors.

A different approach to producing thin zeolite-containing coatings used electrodeposition at a Pt or glassy carbon containing rotating disk electrode (RDE).[25] *Murray* et al. prepared the zeolite-coated RDE by spinning a Pt or glassy carbon RDE in a solution containing powdered zeolite A, Et_4NClO_4/CH_3CN and an oxidant species (1,3-dinitrobenzene, 1,4-dinitrobenzene or tetracyanoquinodimethane). A coating was formed upon repetitive scanning through the reduction waves of the oxidant. The embedded zeolite particles retained their molecular sieving properties. The coating thickness could be increased for organic oxidants by cycling through the second reduction wave and generating a dianion.

In order to use silver sodalites as optical data storage materials, *Stein*[48] embedded sodalites in a polymethylmethacrylate (PMMA) matrix and prepared thin films of the zeolite/polymer composite. This application differs from the above examples in the fact that direct access of gases or other chemicals to the zeolite is *not* required, nor even desirable. The sodalite was ground, sieved and stirred into a toluene/PMMA mixture to achieve a uniform distribution. A thin film was applied on a fused silica disk or similar support and was allowed to dry and cure at room temperature, before being treated near the glass temperature

of PMMA. The hard, highly transparent amorphous polymer PMMA was chosen because its refractive index matched that of sodalite very closely, so that light scattering was minimized. Although individual particles remained visible in many samples, greater control over the mixing and the sodalite particle size should yield fairly homogeneous films.

13. Conclusion

The unique advantages of zeolites are obvious. The stage is therefore set for some rapid and significant developments involving the synthesis, characterization and structure-property relationships of zeolite based electronic, optical, magnetic and dielectric materials. Zeolites, like any other solid state materials, have their limitations. Those specific to zeolites include pore plugging, poisoning, structural defects, the difficulties of growing large single crystals, and interfacing a zeolite device with the outside world. Many of these problems can however, be solved and are deemed to be interesting research projects.

Much of the research involving new applications for zeolite materials is still at a fairly early stage, but one can extrapolate from the present trends to make the following conjectures: the recent discovery of all-silica zeolites will pave the way to zeolite semiconductors; the marked proton conductivity of certain acid zeolites makes possible the fabrication of electrochromic zeolites; the unveiling of acentric zeolites allows the design of zeolite piezoelectric devices; the molecule size pore and channel structure of zeolites provides a novel medium in which to create ultrahigh resolution images and package and process information at high storage densities; the unidimensional channel architecture of certain zeolites permits the assembly of low dimensional zeolite conductors and the control of energy transfer and energy migration in restricted dimensions. All of this implies that innovation in zeolite materials science is likely to burgeon and flourish in the near future.

Received: December 20, 1988

[1] R. M. Barrer: *Hydrothermal Chemistry of Zeolites*, Academic Press, New York 1972.
[2] J. M. Newsam, *Science 231* (1986) 1093; J. M. Thomas, *Angew. Chem. 100* (1988) 1735; *Angew. Chem. Int. Ed. Engl. 27* (1988) 1673.
[3] M. D. Baker, G. A. Ozin, J. Godber, *Catal. Rev.-Sci. Eng. 27* (1985) 591; G. Engelhardt, D. Michel: *High Resolution Solid-State NMR of Silicates and Zeolites*, Wiley, Chichester 1987; C. Baerlocher, *Zeolites 6* (1986) 325.
[4] A. Dyer, S. A. Malik, A. Araya, T. J. McConville in P. A. Williams, M. J. Hudson (Eds.): *Recent Developments in Ion Exchange*, Elsevier, Amsterdam 1987, p. 257.
[5] W. P. Halperin, *Rev. Mod. Phys. 58* (1986) 533.
[6] a) V. Narayanamurti, *Science 235* (1987) 1023; K. Ploog, *Angew. Chem. 100* (1988) 611; *Angew. Chem. Int. Ed. Engl. 27* (1988) 593; b) M. Tsuchiya, J. M. Gaines, R. H. Yan, R. J. Sinies, P. O. Holtz, L. A. Coldren, P. M. Petroff, *Phys. Rev. Lett. 1989*, 466; M. A. Reed, J. N. Randall, R. J. Aggarwal, R. J. Motyi, T. M. Moore, A. E. Wetsel, *Phys. Rev. Lett. 1988*, 535.
[7] J. N. Randall, M. A. Reed, T. M. Moore, R. J. Matyi, J. W. Lee, *J. Vac. Sci. Technol. B6* (1988) 302.
[8] H. Temkin, G. J. Dolan, M. B. Panish, S. N. G. Chu, *Appl. Phys. Lett. 50* (1987) 413.
[9] L. Brus, *J. Phys. Chem. 90* (1986) 2555.
[10] O. Terasaki, K. Yamazaki, J. M. Thomas, T. Ohsuna, D. Watanabe, J. V. Sanders, J. C. Barry, *Nature 330* (1987) 58.
[11] Y. Wang, N. Herron, *J. Phys. Chem. 92* (1988) 4988.
[12] N. Herron, Y. Wang, M. M. Eddy, G. D. Stucky, D. E. Cox, K. Moller, T. Bein, *J. Am. Chem. Soc.* 111 (1989) 530.
[13] Y. Wang, N. Herron, *J. Phys. Chem. 91* (1987) 257.
[14] K. Moller, M. Eddy, G. D. Stucky, N. Herron, T. Bein, *J. Am. Chem. Soc.*, submitted.
[15] G. A. Ozin, A. Stein, G. D. Stucky, J. P. Godber, *J. Inclusion Phenom.*, in press; G. A. Ozin, J. P. Godber, A. Stein, *U. S. Pat.*, Filed August 1988.
[16] V. N. Bogomolov, S. V. Kholodkevich, S. G. Romanov, L. S. Agroskin, *Solid State Commun. 47* (1983) 181.
[17] K. Tamura, S. Hosokawa, H. Endo, S. Yamasaki, H. Oyanagi, *J. Phys. Soc. Jpn. 55* (1986) 528.
[18] J. B. Parise, J. E. MacDougall, N. Herron, R. Farlee, A. W. Sleight, Y. Wang, T. Bein, K. Moller, L. M. Moroney, *Inorg. Chem. 27* (1988) 221.
[19] T. Bein, P. Enzel, *Nature*, submitted.
[20] P. M. McManus, R. J. Cushman, S. C. Yang, *J. Phys. Chem. 91* (1987) 744.
[21] T. Bein, P. Enzel, *Synth. Metals*, in press.
[22] Z. Li, C. Lai, T. E. Mallouk, *Inorg. Chem. 28 (1989)* 178.
[23] J. S. Krueger, J. E. Mayer, T. E. Mallouk, *J. Am. Chem. Soc. 110* (1988) 8232.
[24] N. Petranovic, M. Susic, *Zeolites 3* (1983) 271.
[25] C. G. Murray, R. J. Nowak, D. R. Rolison, *J. Electroanal. Chem. 164* (1984) 205.
[26] D. R. Rolison, E. A. Hayes, R. J. Nowak, S. Pons, M. Fleischmann, *J. Phys. Chem.*, in press.
[27] Z. Li, T. E. Mallouk, *J. Phys. Chem. 91* (1987) 643.
[28] M. Fleischmann, J. Ghoroghchian, S. Pons, *J. Phys. Chem. 89* (1985) 5530; M. Fleischmann, J. Ghoroghchian, D. R. Rolison, S. Pons, *J. Phys. Chem. 90* (1986) 6392.
[29] D. R. Rolison, R. J. Nowak, S. Pons, J. Ghoroghchian, M. Fleischmann, *J. Phys. Chem.*, in press.
[30] L. Persaud, A. J. Bard, A. Campion, M. A. Fox, T. E. Mallouk, S. E. Webber, J. M. White, *J. Am. Chem. Soc. 109* (1987) 7309.
[31] Z. Li, C. M. Wang, L. Persaud, T. E. Mallouk, *J. Phys. Chem. 92* (1988) 2592.
[32] B. De Vismes, F. Bedioni, J. Devynck, C. Bied-Charreton, *J. Electroanal. Chem. 187* (1985) 197; B. De Vismes, F. Bedioni, J. Devynck, C. Bied-Charreton, M. Perrée-Fauvet, *Nouv. J. Chim. 10* (1986) 81.
[33] K. E. Creasy, B. R. Shaw, *Electrochim. Acta 33* (1988) 551.
[34] B. R. Shaw, K. E. Creasy, *J. Electroanal. Chem. 243* (1988) 209.
[35] D. C. Freeman, Jr., US-Pat. 3 186 875, 1965.
[36] W. J. Mortier, R. A. Schoonheydt, *Prog. Solid State Chem. 16* (1985) 1.
[37] E. Krogh Anderson, I. G. Krogh Anderson, E. Skou, S. Yde-Andersen, *Solid State Ionics 18/19* (1986) 1170.
[38] M. M. Thackeray, J. Coetzer, *Solid State Ionics 6* (1982) 135.
[39] M. D. Ingram, C. A. Vincent, *Chem. Br. 20* (1984) 235.
[40] Y. Masumoto, *Jpn. Pat.*, Application May 1985.
[41] B. Sulzberger, G. Calzaferri, *J. Photochem. 19* (1982) 321.
[42] H. Otsuki, M. Kobayashi, Y. Usami, *Jpn. Pat.*, Application August 1985.
[43] A. Bellomo, A. DeRobertis, D. DeMarco, *Inquinamento 22* (1980) 47.
[44] a) G. A. Ozin, M. Baker, A. Kuperman, H. Wiggenhauser, M. M. Olken, E. Flanigen, P. Caughlin, W. Mercer, *U. S. Pat.*, Filed August 1988; b) M. Baker, M. M. Olken, G. A. Ozin, G. A. Ozin, *J. Am. Chem. Soc. 110* (1988) 5709; c) G. A. Ozin, A. Kuperman, E. Flanigen, H. Wiggenhauser, W. Mercer, P. Caughlin, Final Report "Zeolite Chemical Sensors", Union Carbide, Tarrytown 1988.
[45] S. D. Cox, T. E. Gier, G. D. Stucky, J. Bierlein, *J. Am. Chem. Soc. 110* (1988) 2986.
[46] T. Bein, R. F. Carver, R. D. Farlee, G. D. Stucky, *J. Am. Chem. Soc. 110* (1988) 4546.
[47] T. Bein, K. Brown, P. Enzel, C. J. Brinker in *Better Ceramics Through Chemistry III*, MRS Proceedings, in press.
[48] A. Stein, *M. Sc. Thesis*, University of Toronto 1988.
[49] W. M. Meier, D. H. Olson, *Atlas of Zeolite Structure Types*, Structure Commission of the International Zeolite Association 1978.